J|A|C|S
A R T I C L E S

Activation Barriers in the Homolytic Cleavage of Radicals and Ion Radicals

Cyrille Costentin, Marc Robert, and Jean-Michel Savéant*

Contribution from the Laboratoire d'Electrochimie Moléculaire, Université de Paris 7 - Denis Diderot, Case Courrier 7107, 2 place Jussieu, 75251 Paris Cedex 05, France

Received June 13, 2002 ; E-mail: saveant@paris7.jussieu.fr

Abstract: As revealed by several experimental examples, radicals and ion radicals may, in contrast with closed-shell molecules, undergo exothermic homolytic cleavages (·A··B → A: + ·B) with substantial activation barriers. A two-state semiclassical model is proposed for explaining the existence of the barrier and estimating its magnitude. It is based on the intersection of the potential energy surfaces characterizing the dissociation of a bonding state, ·A··B → ·A· + ·B, on one hand, and the approach to bonding distance of a repulsive state, A: + ·B → A∴B, on the other. After inclusion of the bond cleavage and formation as Morse curves in the normal-mode analysis, a simple activation driving force relationship is obtained, the two main ingredients of the intrinsic barrier being the triplet excitation energy of the A moiety and the $\pi^* \rightarrow \sigma^*$ excitation energy in ·A–B. The model is then tested by quantum chemical calculations, first on a simplified system to evaluate the calculation techniques and then on a real system. A comparison of the model predictions with experiment is finally performed using the rate data recently gathered for the cleavage of 4-cyanophenyl alkyl ether anion radicals, which cover a respectable range of driving forces, showing satisfactory agreement between theoretical predictions and experimental data.

Although electron-transfer reactions may lead to chemically stable species, there is a wide variety of instances where injection or removal of one electron into or from a molecule triggers drastic changes in the nuclear framework, as drastic as bond cleavage and bond formation. The interest in this area of electron-transfer chemistry is two-fold. One is that a wealth of reactions can be triggered in this way,[1a] which associates radical and acid−base (in the general sense) reactions to electron transfer.[1b] Besides photolysis and thermolysis, this is a conspicuous route to radical chemistry, with, in many cases, the advantage of a better control of the reactivity. The second aspect is more fundamental in nature. The understanding of the effects of injecting one electron into (or removing one electron from) a molecular edifice is a crucial milestone en route to a general comprehension of chemical reactions where the reshuffling of electrons involves breaking and formation of bonds. It is remarkable in this connection that general reactivity models have been built for electron-transfer reactions with more success than for other, more complex, reactions.[2] Besides the synthetic opportunities deriving from the large diversity of reactions that may be triggered by single electron transfers and the contribution to the fundamentals of chemical reactivity,

two other domains of application should be mentioned. One involves the transduction of the presence of a molecule into an electrochemical signal, that is, the area of sensors, including biosensors.[3] The other is more prospective: if redox centers connected by molecular wires are to play a role in future developments of molecular electronics, the understanding of the structural changes they may undergo upon electron transfer will be central to the design and operation of such devices.[4]

Among the reactions accompanying electron transfer, particular attention has been devoted to bond cleavage, whether the initial electron transfer to a molecule forms a frangible species that cleaves in a successive step or leads directly to products in a concerted process.[2e] In the case of a stepwise mechanism, and starting with a closed-shell molecule, a high energy primary radical resulting from single electron transfer is first formed, which generally cleaves more readily than its parent. Thus, starting from a radical or an ion radical that we note AB·, two cases may be distinguished according to the location of the unpaired electron (Scheme 1). In the heterolytic case, the unpaired electron is mostly located on the B portion of the molecule. The cleavage of the bond that forms A and B· involves an intramolecular electron transfer from the B to the A moieties in the case where the radical or ion radical results from a reduction and an intramolecular electron transfer in the reverse direction in the case where it comes from an oxidation.[5]

(1) (a) *Organic Electrochemistry*; Lund, H., Baizer, M. M., Eds.; Dekker: New York, 1990. (b) Andrieux, C. P.; Savéant, J.-M. Electrochemical Reactions. In *Investigations of Rates and Mechanisms of Reactions*; Bernasconi, C. F., Ed.; Wiley and Sons: New York, 1986; Vol. 6, 4/E, Part 2, C; pp 305−390.

(2) (a) Marcus, R. A. *J. Chem. Phys.* **1956**, *24*, 4966. (b) Hush, N. S. *J. Chem. Phys.* **1958**, *28*, 962. (c) Marcus, R. A. In *Special Topics in Electrochemistry*; Rock, P. A., Ed.; Elsevier: New York, 1977; pp 161−179. (d) Marcus, R. A. *Faraday Discuss. Chem. Soc.* **1982**, *74*, 7. (e) Savéant, J.-M. Single Electron Transfer and Nucleophilic Substitution. In *Advances in Physical Organic Chemistry*; Tidwell, T. T., Ed.; Academic Press: New York, 2000; Vol. 35, pp 117−192.

(3) Turner, A. P. F.; Karube, I.; Wilson, G. S. *Biosensors. Fundamentals and Applications*; Oxford University Press: New York, 1987.

(4) (a) *Molecular Electronics: Science and Technology*; Aviram, A., Ratner, M., Eds.; New York Academy of Sciences: New York, 1998. (b) Joachim, C.; Gimzewski, J. K.; Aviram, A. *Nature* **2000**, *408*, 541. (c) Fox, M. A. *Acc. Chem. Res.* **1999**, *32*, 201.

Scheme 1. Heterolytic and Homolytic Cleavage of a Radical or Ion Radical Resulting from a Reduction (Left) or an Oxidation (Right)

Scheme 2. Examples of Exothermic Homolytic Cleavage of Radicals and Ion Radicals
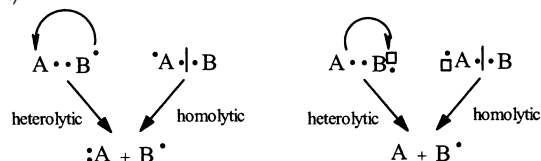
In the second case, the unpaired electron is located on the A portion of the molecule. The cleavage of the bond that forms A and B• involves a homolytic scission of the A−B bond.[5] A two-state model, based on an intramolecular version of the Morse-curve model of dissociative electron transfer,[6a] has been proposed,[6b] for both the heterolytic and the homolytic mode of cleavage. The application of this model does not seem to raise major difficulties in the first case insofar that heterolytic cleavage of ion radicals has been conceived as an intramolecular electron-transfer process for a long time.[6b,7] This is far less obvious in the case of a homolytic cleavage. In addressing this question, precious hints come from experimental studies. In a number of cases, it has been found that the homolytic cleavage of both cation and anion radicals into a radical and an ion is endothermic with a small barrier, if any, for the reverse reaction.[8] These observations seem to indicate that homolytic dissociation of radicals into another radical and a closed-shell molecule follows the same Morse curve behavior as the dissociation of closed-shell molecules into two radicals on which the derivation of thermodynamic data from kinetic measurements is based.[9] One would thus predict that substrates giving rise upon reduction or oxidation to exothermically cleaving radicals should necessarily undergo a concerted dissociative electron-transfer reaction. However, several reports provide evidence that this behavior is not general and that exothermic cleavage of radicals may exhibit a significant activation barrier. One example is provided by the electrochemical reduction of *tert*-butylperbenzoates,[10] where a transition between stepwise and concerted mechanisms has been observed upon changing either the para-substituent on the phenyl ring or the driving force of the reaction by means of the cyclic
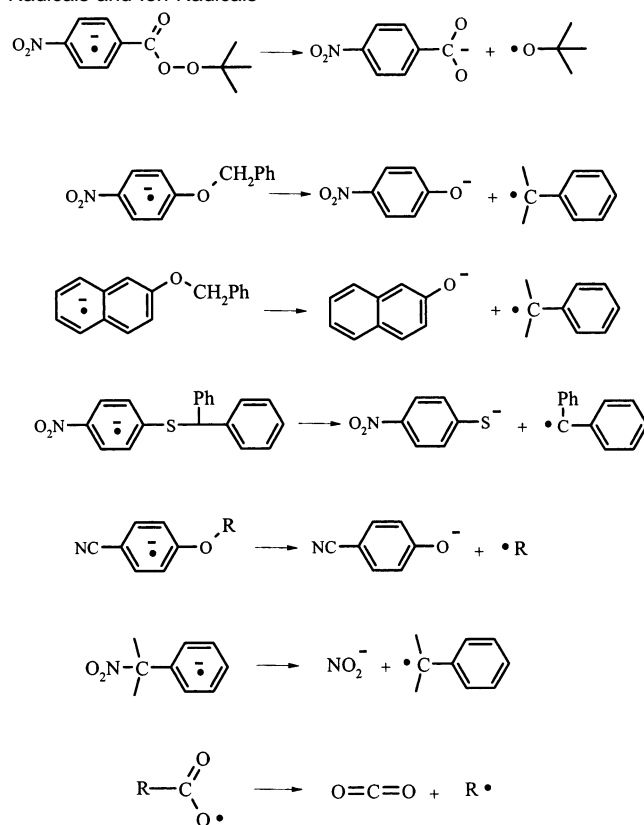
voltammetric scan rate. In the latter case, that is, with the 4-nitro-derivative, the cleavage of the O−O bond in the anion radical (Scheme 2) is exothermic. Other studies have shown that the anion radicals of nitrobenzyl phenyl ether,[11a] naphthylmethyl phenyl ether,[11b] nitrophenyl diphenylmethyl thioether,[11c] and a series of cyanophenyl alkyl ethers[11d] also undergo an exothermic homolytic cleavage that possesses a sizable activation barrier (Scheme 2).[11e] Another example involves the cleavage of the anion radical of α-nitrocumyl, yielding the nitrite ion and the cumyl radical (Scheme 2).[12] Still another example, concerning a neutral radical rather than an ion radical, is provided by the Kolbe reaction[13a,b] where the intermediary acyloxy radical[13c] also undergoes an exothermic homolytic fragmentation (Scheme 2).[13d]

(5) For the sake of simplicity and generality, the charges borne by the radical and fragments have been omitted. AB• can be an anion, a cation, or a neutral radical. If the parent molecule AB is a neutral molecule, its reduction indeed yields an anion radical, and its oxidation yields a cation radical, producing in both cases a neutral radical B• and a closed-shell molecule A, which is an anion in the reduction case and a cation in the oxidation case. AB• can as well be a neutral radical resulting either from the reduction of a cationic substrate or from the oxidation of an anionic substrate, producing a neutral secondary radical, B•, and a neutral leaving group, A.
(6) (a) Savéant, J.-M. *J. Am. Chem. Soc.* **1987**, *109*, 6788. (b) Savéant, J.-M. *J. Phys. Chem.* **1992**, *96*, 3716.
(7) (a) Neta, P.; Behar, D. *J. Am. Chem. Soc.* **1980**, *102*, 4798. (b) Neta, P.; Behar, D. *J. Am. Chem. Soc.* **1981**, *103*, 103. (c) Behar, D.; Neta, P. *J. Am. Chem. Soc.* **1981**, *103*, 2280. (d) Rossi, R. A. Z. *Naturforsch.* **1984**, *A39*, 1984. (e) Andrieux, C. P.; Savéant, J.-M.; Zann, D. *Nouv. J. Chim.* **1984**, *8*, 107.
(8) (a) Anne, A.; Fraoua, S.; Moiroux, J.; Savéant, J.-M. *J. Am. Chem. Soc.* **1996**, *118*, 3938. (b) Maslak, P.; Vallombroso, T. M.; Chapmann, W. H.; Narvaez, J. N. *Angew. Chem., Int. Ed. Engl.* **1994**, *33*, 73. (c) Maslak, P.; Narvaez, J. N.; Vallombroso, T. M.; Watson, B. A. *J. Am. Chem. Soc.* **1995**, *117*, 12380. (d) Maslak, P.; Chapmann, W. H.; Vallombroso, T. M. *J. Am. Chem. Soc.* **1995**, *117*, 12373. (e) This assertion is supported by the observation that the overall reaction is controlled by the diffusion of the two fragments out of the solvent cage, the cleavage step acting as a preequilibrium, as revealed by the F/RT slope of the ln k versus driving force plot.[8a] The smallness of the activation barrier of the bond-forming reaction is thus attested by the fact that this reaction is faster than the diffusion of the two fragments out of the solvent cage.
(9) (a) Glasstone, S.; Laidler, K.; Eyring, H. *The Theory of Rate Processes*; McGraw-Hill: New York, 1941. (b) Laarhoven, L. J. J.; Born, J. G. P.; Arends, I. W. C. E.; Mulder, P. *J. Chem. Soc., Perkin Trans. 2* **1997**, 2307.
(10) Antonello, S.; Maran, F. *J. Am. Chem. Soc.* **1999**, *121*, 9668.

(11) (a) Maslak, P.; Guthrie, R. D. *J. Am. Chem. Soc.* **1986**, *108*, 2628. (b) Maslak, P.; Guthrie, R. D. *J. Am. Chem. Soc.* **1986**, *108*, 2637. (c) Maslak, P.; Theroff, J. *J. Am. Chem. Soc.* **1996**, *118*, 7235. (d) Andrieux, C. P.; Farriol, M.; Gallardo, I.; Marquet, J. *J. Chem. Soc., Perkin Trans. 2* **2002**, *2*, 985. (e) Examination of the cleavage kinetics of the anion radicals of the nitro-substituted ethers and thioethers[11a−c] involved the comparison of the kinetics of homolytic and heterolytic cleavages and led to the statement of an empirical "spin regioconservation principle" according to which the activation barrier is the smallest for the reaction in which the unpaired electron remains on the same side of the anion radical molecule upon cleavage.[11a,b] In fact, the rule is not connected to the electron spin,[11f] but has rather been proposed to be the result of the transition state being more polar in the heterolytic case than in the homolytic case.[11a−c,f] The effects are small which makes reliable quantum chemical analyses difficult, leading to the impression that presently available experimental and theoretical evidence is too scarce to ascertain the generality of the rule and of its putative explanation. (f) Pisano, L.; Farriol, M.; Asensio, X.; Gallardo, I.; Gonzalez-Lafont, A.; Lluch, J. M.; Marquet, J. *J. Am. Chem. Soc.* **2002**, *124*, 4708.
(12) Zheng, Z.-R; Evans, D. H.; Soazara Chan-Shing, E.; Lessard, J. *J. Am. Chem. Soc.* **1999**, *121*, 9429.
(13) (a) Kolbe, H. *Ann. Chem.* **1849**, *69*, 257. (b) Wurtz, A. *Ann. Chim. Phys.* **1855**, *44*, 291. (c) Andrieux, C. P.; Gonzalez, F.; Savéant, J.-M. *J. Electroanal. Chem.* **2001**, *498*, 171. (d) Hilborn, J. H.; Pincock, J. A. *J. Am. Chem. Soc.* **1991**, *113*, 7158.
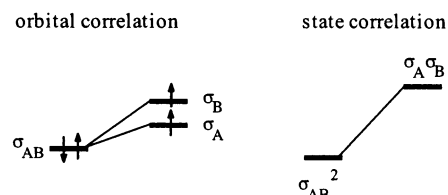
Figure 1. Homolytic cleavage of a closed-shell molecule. Orbital and state correlation diagrams.

The purpose of the work reported below was an attempt to understand what are the fundamental reasons that homolytic cleavage of radicals or ion radicals may possess, unlike closed-shell molecules, a sizable activation barrier, and propose a quantitative model able to reproduce reasonably well existing experimental data. The discussion will go successively through the following steps: (i) Orbital and energy description of pertinent diabatic states for a two-state model of the reaction dynamics; (ii) extension of the notion of vibration normal modes to cleavage normal modes and derivation of the model key equations; (iii) testing the model by quantum chemical calculations on a simplified system and evaluation of the calculation techniques; (iv) testing the model by quantum chemical calculations on a real system; and (v) comparison with experiment using the rate data recently gathered for the cleavage of 4-cyanophenyl alkyl ether anion radicals, which cover a significant range of driving forces.[11]

Orbital and Energy Description of Pertinent Diabatic States in the Homolytic Cleavage of Radicals or Ion Radicals

In the homolytic cleavage of a closed-shell molecule, orbital correlation between reactant and products entails a single electronic state (Figure 1).[14] As the bond stretches, it acquires a diradical character yielding a radical pair when the bond is cleaved.[15] In the search for a two-state description of the reaction dynamics of the homolytic cleavage of radicals or ion radicals, we first consider the simplest case, that is, the case of an A−B molecule with a π system on the A moiety and no overlap between this π system and the orbitals describing the scissile bond. Using a minimal set of orbitals (Figure 2), we describe the reactant by the orbitals σ_{AB} and σ_{AB}* of the scissile bond and a π-type orbital labeled π_{AB}*, which corresponds to a bonding, antibonding, or nonbonding orbital if AB· is a cation, anion, or neutral radical, respectively. For the products, the minimal set of orbitals includes two σ-type orbitals labeled n_A and p_B and a π-type orbital labeled π_A*, which corresponds to a bonding, antibonding, or nonbonding orbital if A is a cation, anion, or neutral radical, respectively. The ground state of the reactant state **R** corresponds to an electronic configuration $[\sigma_{AB}^2\pi_{AB}*]$. When the A−B bond dissociates homolytically, the σ_{AB} and σ_{AB}* orbitals correlate with the n_A and p_B orbitals, while the π_{AB}* orbital correlates with the π_A* orbital. It follows that, as shown in Figure 2 (left), at the product geometry, the state **R** corresponds to the electronic configuration $[n_A p_B \pi_A *]$. This is an excited state of the product system **P**, which possesses, in its ground state, a $[n_A^2 p_B]$ electronic configuration. In other words, in state **R** at the product geometry, the fragment B is in its fundamental configuration, as it is in the product ground
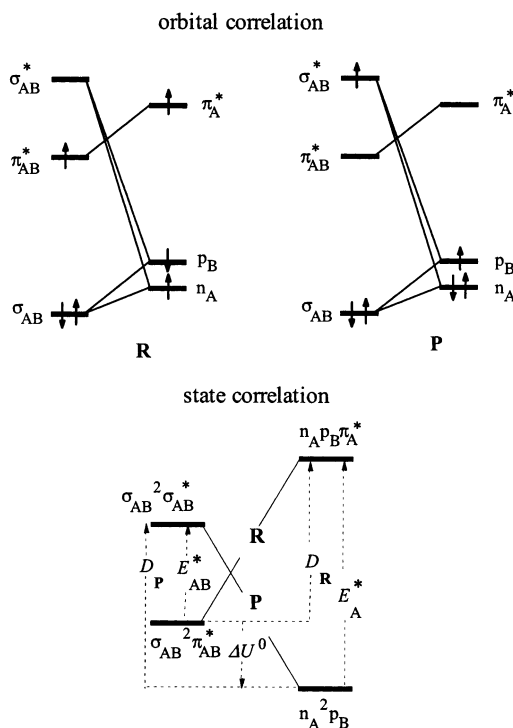
(14) Shaik, S. S.; Shurki, A. *Angew. Chem., Int. Ed.* **1999**, *38*, 586.
(15) Dauben, W. G.; Salem, L.; Turro, N. J. *Acc. Chem. Res.* **1975**, *8*, 41.

Figure 2. Homolytic cleavage of radicals or ion radicals in the case where the π system on the A moiety does not overlap the orbitals of the scissile bond. Orbital and state correlation.

state, while the anion A⁻ lies in a triplet excited state and is the result of a n → π* transition. The homolytic cleavage thus implies that an electron is being transferred from the π_{AB}* orbital to the σ_{AB}* orbital. Strictly speaking, this electronic transition is forbidden because it has been assumed that these two orbitals do not overlap. In practice, however, out-of-plane vibrations will make the two states mix in most cases, thus allowing the passage between the diabatic states **R** and **P** at the transition state.

The homolytic dissociation energy of the A−B bond of the AB· radical along the reactant diabatic curve, that we note D_R, may thus be related to the triplet excitation energy, E_A^*, according to eq 1.

$$D_R = E_A^* + \Delta U^0 \qquad (1)$$

where ΔU^0 is the energy difference between product and reactant at equilibrium geometry.

Along the product diabatic curve, the energy required to put the two fragments in the geometry they have in the reactant ground state, D_P, is related to the π* → σ* excitation energy, E_{AB}^*, according to eq 2.

$$D_P = E_{AB}^* - \Delta U^0 \qquad (2)$$

We now address another case where the π system on the A moiety can overlap the σ_{AB} and σ_{AB}* orbitals of the breaking bond. Orbital correlation is as shown in Figure 3, taking into account that, as the cleavage proceeds, the σ-like and π-like orbitals mix to produce $\pi_{A,1}$ to $\pi_{A,3}$ orbitals, on one hand, and p_B, on the other. Construction of the state correlation diagrams is not as straightforward as in the preceding case because there is no strict distinction between the π and σ orbitals. The appropriate procedures are detailed in the Supporting Informa-

orbital correlation
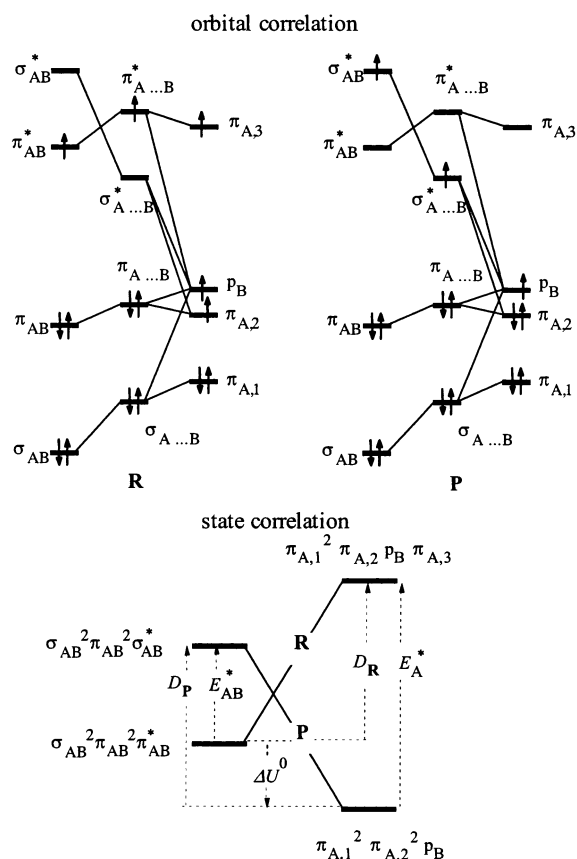
state correlation

Figure 3. Homolytic cleavage of radicals or ion radicals in the case where the π system on the A moiety overlaps the orbitals of the scissile bond. Orbital and state correlation diagrams.

tion, leading to the diagrams in Figure 3. The $[\sigma_{AB}{}^2\pi_{AB}{}^2 \pi_{AB}{}^*]$ electronic configuration of the **R** ground state is correlated to a $[\pi_{A,1}{}^2\pi_{A,2}p_B\pi_{A,3}]$ configuration at the product geometry. This is an excited state of the product **P** at equilibrium geometry (electronic configuration: $[\pi_{A,1}{}^2\pi_{A,2}{}^2p_B]$), corresponding to a $\pi \rightarrow \pi^*$ transition in the A moiety from the ground state to the triplet state, while B remains in its ground-state configuration. It follows that, as in the preceding case, the homolytic cleavage thus implies that an electron is being transferred from the $\pi_{AB}{}^*$ orbital to the $\sigma_{AB}{}^*$ orbital, with a mixing of the two electronic states at the transition state. The difference is that there is no symmetry restriction opposing the mixing of the two orbitals. Therefore, the resonance (or avoided crossing) energy should not be considered a priori as negligible in the derivation of the activation energy in a model based on the application of eqs 1 and 2.

An example of this type of radical cleavage is provided by the fifth reaction in Scheme 2 (see Illustrating the Model section).

A Two-State Model of the Homolytic Cleavage of Radicals and Ion Radicals

Cleavage Normal Modes and Derivation of the Activation Barrier. The state correlation diagram in Figures 2 and 3 suggests a two-state model of the reaction dynamics based on the intersection of the potential energy surfaces characterizing the dissociation of a bonding state, $\cdot A \cdot \cdot B \rightarrow \cdot A \cdot + \cdot B$, on one hand, and the approach to bonding distance of a repulsive state, $A: + \cdot B \rightarrow A \therefore B$, on the other. Bond cleavage and formation

may be included in the analysis of normal modes as follows. In a closed-shell molecule A−B, containing n atoms, there are $3n$ Cartesian coordinates x_j and $N = 3n - 6$ internal coordinates r_j. Mass-weighted Cartesian displacement coordinates X_j are defined as $X_j = \sqrt{m_j}\Delta x_j$. When rotation and vibration are treated as harmonic motions, N harmonic normal modes, characterized by their fundamental frequencies, ν_j, can be defined. There is one normal coordinate Q_j associated with each normal mode and vice versa. The normal coordinates are derived from the mass-weighted Cartesian displacement coordinates X_j by means of linear equations so that the dependence of the potential energy U from the normal coordinates involves no cross products but only squares:

$$U = U(AB) + \frac{1}{2}\sum_j 4\pi^2\nu_j^2 Q_j^2$$

where $U(AB)$ is the potential energy of A−B at ground-state equilibrium geometry.[16]

In the modeling of the cleavage of a radical or ion radical $\cdot A - B$, the motion along the A−B bond in the $\cdot A \cdot \cdot B$ bonding state is not harmonic. It may be represented by a Morse curve,[6] thus suggesting the replacement of the corresponding internal coordinate r_{AB} (bond length) by the coordinate:

$$Z = \frac{1 - \exp[-\beta(r_{AB} - r_{AB}^0)]}{\beta}$$

where β is the shape factor, and r_{AB}^0 is the value of r_{AB} at equilibrium geometry. The coupling with the other coordinates may thus be treated similarly to the case of a closed-shell molecule, leading to the determination of the normal coordinates q_j and to a quadratic expression of the potential energy (see Supporting Information):

$$U^R = U(\cdot AB) + \frac{1}{2}\sum_j 4\pi^2\nu_j^2 q_j^2 \qquad (3)$$

The other, nonbonding, state involved corresponds to the product system. The approach of the two fragments A and B· from infinite to bonding distance is assumed to be purely repulsive, in line with the fact that the electronic configuration of the fragments, three electrons and two interacting orbitals (or five electrons and four interacting orbitals), does not allow a bonding interaction. The variation of the potential energy with the internal coordinate r_{AB} is classically assumed to be the same as the repulsive part of the reactant Morse curve.[6] It is also assumed that the force constants corresponding to motions inside the A and B· fragments remain the same as those in the AB· molecule. Under these assumptions, the normal coordinates are the same as for the reactant system, and the potential energy is given by (see Supporting Information):

$$U^P = U(A + B^\bullet) + \frac{1}{2}\sum_j 4\pi^2\nu_j^2(q_j - q_j^P)^2 \qquad (4)$$

where $U(A + B^\bullet)$ is the potential energy of the fragments at

(16) Wilson, E. B.; Decius, J. C.; Cross, P. C. *Molecular Vibrations: The Theory of Infrared and Raman Vibrational Spectra*; Dover Publications: New York, 1955.

infinite distance, the geometry being then characterized by the normal coordinates value q_j^P (see Supporting Information).

In the case where the π system on the A moiety does not overlap the orbitals of the scissile bond (see preceding section), the activation barrier, $\Delta U^\ddagger$, may be derived from the saddle point on the intersection of the two zero-order quadratic potential energy surfaces defined by eqs 3 and 4:

$$\Delta U^\ddagger = \frac{\lambda_i}{4}\left(1 + \frac{\Delta U^0}{\lambda_i}\right)^2 \quad \text{with} \quad \lambda_i = \sum_j \lambda_j = \sum_j 2\pi^2 \nu_j^2 \Delta q_j^2 \tag{5}$$

(Δq_j is the variation of q_j from initial to final geometry). The assumption made above implies that D_R and D_P defined in eqs 1 and 2 are equal; then

$$\lambda_i = D_R = D_P$$

In fact, as seen further on, this is not exactly true in a number of cases. A reasonable approximation then consists of using an average value:

$$\lambda_i = \frac{D_R + D_P}{2} = \frac{E_A^* + E_{AB}^*}{2} \tag{6}$$

In the case where the π system on the A moiety overlaps the orbitals of the scissile bond, the resonance (or avoided crossing) energy, H, at the transition state should be taken into account, leading to replacement of eq 5 by:

$$\Delta U^\ddagger = \frac{\lambda_i}{4}\left(1 + \frac{\Delta U^0}{\lambda_i}\right)^2 - H \tag{7}$$

For reactions taking place in a solvent phase such as those we are interested in, solvent reorganization should be introduced as an independent contribution to the activation barrier. It stems from the displacement of the center of charges and the change of charge density that attends the reaction. The solvent reorganization energy, λ_0, may then be estimated by Marcus-type charging cycles.[2c] An example will be given in the last section of the paper, when the predictions of the model will be compared with experiment. In this connection, it is useful to convert eqs 5 and 7 by introduction of the activation free energy and the standard free energy of the reaction so as to facilitate the comparison with experimental data. Following previously described procedures,[17] one obtains:

$$\Delta G^\ddagger \cong \frac{\lambda_i + \lambda_0}{4}\left(1 + \frac{\Delta G^0}{\lambda_i + \lambda_0}\right)^2 (-H) \tag{8}$$

Significant interactions between the fragments resulting in the formation of a product cluster (Figure 4) may alter the validity of the above equations calling for a modification of the model. A treatment similar to that already developed for intermolecular dissociative electron transfer[2e,18] applies here too

(17) Andrieux, C. P.; Savéant J.-M.; Tardy, C. *J. Am. Chem. Soc.* **1998**, *120*, 4167.
(18) (a) Pause, L.; Robert, M.; Savéant, J.-M. *J. Am. Chem. Soc.* **2000**, *122*, 9829. (b) Pause, L.; Robert, M.; Savéant, J.-M. *J. Am. Chem. Soc.* **2001**, *123*, 11908.
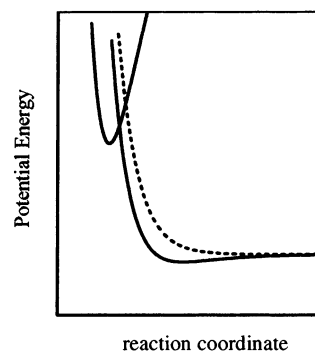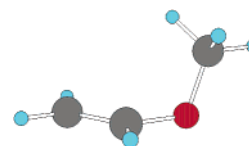
Figure 4. Potential energy curves for bond cleavage and bond formation with (full line) and without (dotted line) interaction between the fragments.

Scheme 3. Geometry of the Constrained Anion Radical of Methyl Vinyl Ether

(see Supporting Information), leading to eqs 9 and 10 in place of eqs 5, 7, and 8.

$$\Delta U^\ddagger = \frac{(\sqrt{\lambda_i} - \sqrt{D_I})^2}{4}\left[1 + \frac{U_0 - D_I}{(\sqrt{\lambda_i} - \sqrt{D_I})^2}\right]^2 \tag{9}$$

$$\Delta G^\ddagger \cong \frac{(\sqrt{\lambda_i} - \sqrt{D_I})^2 + \lambda_0}{4}\left(1 + \frac{\Delta G^0 - \Delta G_I^0}{(\sqrt{\lambda_i} - \sqrt{D_I})^2 + \lambda_0}\right)^2 (-H) \tag{10}$$

where D_I and ΔG_I^0 are the energy and free energy of interaction, respectively. Such interactions are maximal in the gas phase and decrease strongly when going to polar solvents. They may, however, survive under these conditions if the radical fragment possesses a Lewis acid character, induced, for example, by the presence of strong electron-withdrawing substituents.[18]

Illustrating the Model by Quantum Chemical Calculations on a Simplified Test System

The system we selected is the anion radical of methyl vinyl ether, imposing that the vinyl fragment be constrained to remain planar, leading to the optimized structure shown in Scheme 3.

This constraint was imposed for making the model closer to the molecules of practical interest that will be discussed later on, the 4-cyanophenyl alkyl ether anion radicals, than would be the nonconstrained anion radical.

The calculations were performed at both the MP2/6-31G* and the B3LYP/6-31G* levels with no attempt to take solvation into account. Only electronic energy was taken into account. A transition state was localized and characterized, allowing for the determination of the ab initio activation barrier, $\Delta U_{abi}^\ddagger$ (Table 1). The minimum energy path, calculated in mass-weighted internal coordinates (IRC), descends from the transition state structure to the anion radical minimum structure on one side and to a fragment product cluster, somewhat more stable than the separated fragments, on the other side (Figure 5). This cluster is 110 meV more stable than the separated fragments at the B3LYP level and only 5 meV at the MP2 level. It results from an attractive charge-induced dipole interaction which

Table 1. Activation Energies from Quantum Chemical Calculations and from the Predictions of the Model[a]

method	ΔU^0	E_A^*	E_{AB}^*	λ_i	D_I	$\Delta U_{model}^{\ddagger}$ [b]	$\Delta U_{abi}^{\ddagger}$
	Constrained Anion Radical of Methyl Vinyl Ether						
MP2	−1.53	4.20	1.83	3.02	0.005	0.14	0.32 (0.21[c])
B3LYP	−1.22	4.04	1.83	2.94	0.11	0.05	0.10
	Anion Radical of 4-Cyanophenyl Methyl Ether						
B3LYP	−0.20	3.28	2.92	3.10	0.00	0.69	0.56

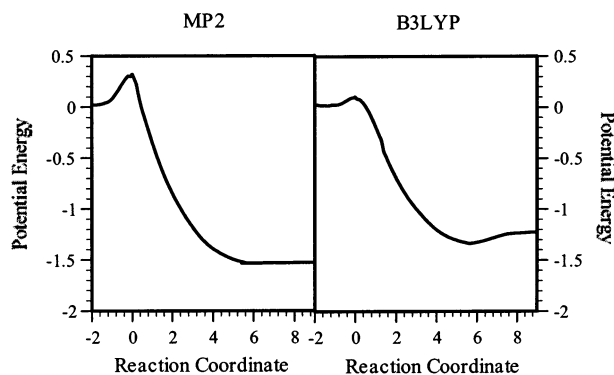[a] All energies in eV. [b] $H = 0$. [c] Projected energy (PMP2).

Figure 5. Homolytic cleavage of the geometrically constrained anion radical of methyl vinyl ether. Intrinsic reaction coordinate profiles from MP2/6-31G* and B3LYP/6-31G* calculations. Reaction coordinate in amu$^{-1/2}$ bohr; potential energy in eV.
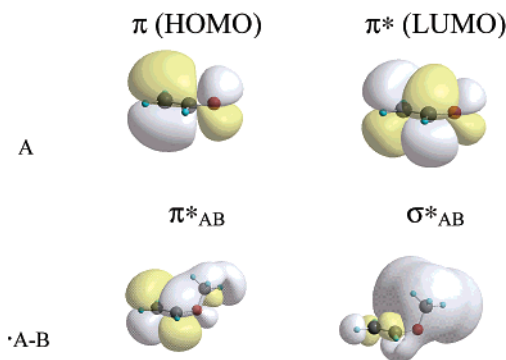

Figure 6. Orbitals involved in the electronic transitions of interest in the vinyl oxide anion and the anion radical of methyl vinyl ether.

should be taken into account in the comparison with the predictions of the model. The predicted activation energy, $\Delta U_{model}^{\ddagger}$, was therefore derived from eq 9 rather than from eq 7, using the values of ΔU^0 and D_I obtained from the MP2 and B3LYP calculations, respectively (Figure 5 and Table 1). The values of E_A^* and E_{AB}^* are needed for estimating the reorganization energy (eq 6).

As discussed in the first section, E_A^* is the energy of a $\pi \rightarrow \pi^*$ transition corresponding to the formation of the first triplet state of CH$_2$CHO$^-$. It corresponds to the passage of an electron from the HOMO to the LUMO orbitals, which are both π-type orbitals as seen in Figure 6. The value thus found for E_A^* is somewhat larger with MP2 than for B3LYP.

E_{AB}^* corresponds to a $\pi^* \rightarrow \sigma^*$ transition as shown in Figure 6. The value obtained in MP2 is unreliable because of massive spin contamination. We thus retained the B3LYP value also for the estimation of $\Delta U_{model}^{\ddagger}$ in the MP2 framework. That we are indeed dealing with a $\pi^* \rightarrow \sigma^*$ transition is confirmed by the fact that the spin density on the CH$_3$ carbon, which is practically nil in the anion radical (0.06, B3LYP), becomes quite

Scheme 4. Optimized Geometry of the Anion Radical of 4-Cyanophenyl Methyl Ether
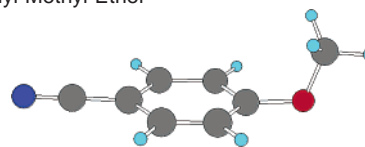
significant in the transition state (0.35, B3LYP). That the electron is transferred to an antibonding orbital is indicated by the substantial stretching of the bond between the anion radical (1.470 Å, B3LYP) and the transition state (1.672 Å, B3LYP).

Coming back to $\Delta U_{abi}^{\ddagger}$, we note that in the MP2 calculation, the spin contamination increases substantially from the reactant ground state to the transition state (S^2 passes from 0.767 to 0.82). Spin contamination is reduced to 0.79 if projected energies are taken into consideration, making $\Delta U_{abi}^{\ddagger}$ pass from 0.32 to 0.21 eV. All results are gathered in Table 1, showing that there is a satisfactory agreement between the predictions of the model and the ab initio results. It should be remarked in this connection that $\Delta U_{model}^{\ddagger}$ corresponding to B3LYP calculations is most probably underestimated because DFT methods are not well suited to the description of anion radicals at large interatomic distances and tend to overestimate cluster stabilization.[19] At the MP2 level, $\Delta U_{abi}^{\ddagger}$ is likely to be somewhat overestimated, even dealing with the projected energy, because of residual spin contamination.

Even taking these uncertainties into account, it is worth noting that, despite the lack of symmetry restrictions, the resonance energy at the transition state does not seem to affect markedly the height of the activation barrier.

Testing the Model by Quantum Chemical Calculations on a Real System

The anion radical of 4-cyanophenyl methyl ether was taken as a representative of the series of compounds that will be used in the next section to test the prediction of the model against experimental results. Because B3LYP/6-31G* calculations were found satisfactory in the study of the preceding simple system, we continued to use the same level of calculation with the present, much larger, system, for which MP2 calculations would be exceedingly time-consuming. Full optimization of the ground state (Scheme 4) revealed that there is an overlap between the planar π system and the σ orbitals of the breaking bond quite similar to the situation found with the simplified system.

The minimum energy path for the homolytic cleavage, calculated in mass-weighted internal coordinates (IRC), is shown in Figure 7, pointing to an activation energy of 0.56 eV and a standard energy of reaction of −0.20 eV (Table 1) and indicating that there is no significant cluster formation on the product side. We thus used eq 7 for estimating $\Delta U_{model}^{\ddagger}$, after estimation of E_A^* and E_{AB}^*. E_A^* is the energy of a $\pi \rightarrow \pi^*$ transition forming the first triplet state of 4-cyanophenyloxide anion. It corresponds to the passage of an electron from the HOMO to the LUMO orbitals, which are both π-type orbitals as seen in Figure 8. E_{AB}^* corresponds to a $\pi^* \rightarrow \sigma^*$ transition as shown also in Figure 8. That we are actually dealing with a $\pi^* \rightarrow \sigma^*$ transition

(19) (a) Sala, F. D.; Görling, A. *J. Chem. Phys.* **2002**, *116*, 5374. (b) Becke, A. D. *J. Chem. Phys.* **2000**, *112*, 4020. (c) Zhang, Y.; Yang, W. *J. Chem. Phys.* **1998**, *109*, 2604. (d) Bally, T.; Sastry, N. *J. Phys. Chem. A* **1997**, *101*, 7923. (e) Chermette, H.; Ciofini, I.; Mariotti, F.; Daul, C. *J. Chem. Phys.* **2001**, *115*, 11068.
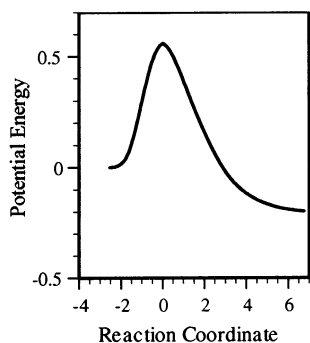
Figure 7. Homolytic cleavage of the anion radical of 4-cyanophenyl methyl ether. Reaction coordinate in $amu^{-1/2}$ bohr; potential energy in eV.

π (HOMO) π^* (LUMO)

A

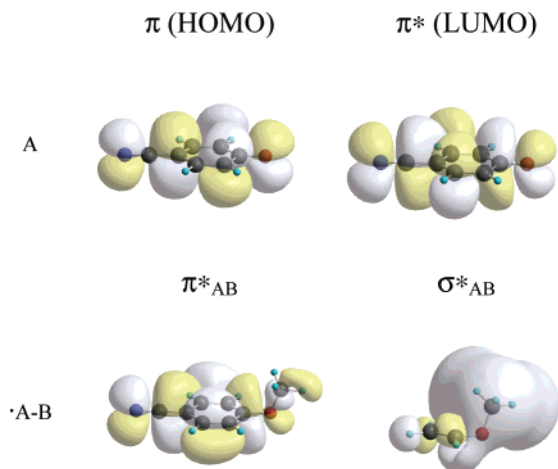π^*_{AB} σ^*_{AB}

$\cdot A\text{-}B$

Figure 8. Orbitals involved in the electronic transitions of interest in the 4-cyanophenyl oxide anion and the anion radical of 4-cyanophenyl methyl ether.

is confirmed by the fact that the spin density on the CH_3 carbon, which is practically nil in the anion radical (0.02, B3LYP), becomes quite significant in the transition state (0.53, B3LYP). The antibonding orbital character of the orbital to which the electron is transferred matches the substantial stretching of the bond between the anion radical (1.415 Å, B3LYP) and the transition state (1.802 Å, B3LYP).

All results are gathered in Table 1, showing that there is a satisfactory agreement between the predictions of the model and the ab initio results. Here again the resonance energy appears to play a minor role, if any.

Comparison with Experiment

We now test the model by comparison with the rate data recently gathered for the cleavage of 4-cyanophenyl alkyl ether anion radicals.[11d]

To the best of our knowledge this is, at present, the only available series of anion radicals undergoing an exergonic homolytic cleavage for which the rate constants have been systematically measured over an extended range of driving forces. The rate constants, k, are converted into activation free energies, $\Delta G^{\ddagger}$, according to

$$k = (k_B T/h) \exp(-F\Delta G^{\ddagger}/RT)$$

(k_B, Boltzmann constant; T, absolute temperature; R, gas constant; F, Faraday) taking $k_B T/h = 5 \times 10^{12}$ s^{-1}, and plotted
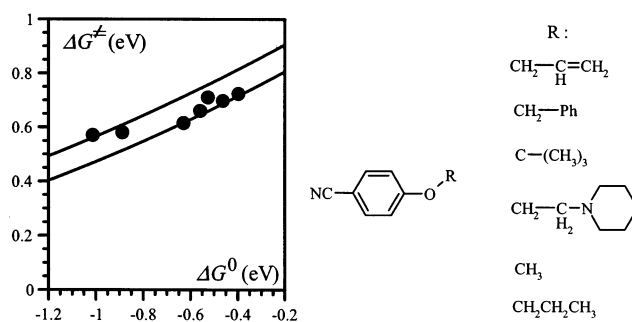

Figure 9. •: Activation free energy of the homolytic cleavage of anion radicals of 4-cyanophenyl alkyl ethers. From left to right: alkyl = allyl, benzyl, *tert*-butyl, ethylpiperidinyl, *i*-butyl, methyl, *n*-propyl. —: Application of the model (see text).

Table 2. Thermodynamics of the Homolytic Cleavage of 4-Cyanophenyl Alkyl Ether Anion Radicals[a]

R	$E^0_{ArOR/ArOR^{\bullet-}}$	$T\Delta S^0_{ArO-R}$	D_{ArO-R}	ΔG^0
allyl	−2.42	0.512	2.48	−1.012
benzyl	−2.39	0.468	2.53	−0.888
t-butyl	−2.36	0.459	2.75[b]	−0.629
ethylpiperidinyl	−2.51	0.479	2.99	−0.559
i-butyl	−2.47	0.487	2.99	−0.527
methyl	−2.47	0.443	3.01	−0.463
n-propyl	−2.47	0.477	3.11	−0.397

[a] Energies in eV; standard potentials in V versus SCE. [b] The pertinent thermochemical data are not available. D_{ArO-R} was obtained from a linear correlation between the thermochemical data and the B3LYP values constructed with the other six compounds.

against the driving force (Figure 9). ΔG^0 is obtained by application of eq 11.

$$\Delta G^0 = D_{ArO-R} - T\Delta S^0_{ArO-R} + E^0_{ArOR/ArOR^{\bullet-}} - E^0_{ArO^{\bullet}/ArO^-} \tag{11}$$

where D_{ArO-R} is the bond dissociation energy in the parent ether, and ΔS^0_{ArO-R} is the attending standard variation of entropy. The E^0's are the standard potentials of the subscript species. The $ArOR/ArOR^{\bullet-}$ standard potentials have been determined experimentally (Table 2),[11d] whereas the $ArO^{\bullet}/ArO^-$ standard potential is 0.56 V versus SCE.[20] The standard variation of entropy was obtained from thermochemical tables,[21] using 3.25 meV K^{-1}, for the entropy of formation of $ArO^{\bullet}$.[22] The bond dissociation energies are calculated from thermochemical tables,[21] or from the NIST database, using:

$$D_{ArO-R} = \Delta_f H_{R^{\bullet}} + \Delta_f H_{ArO^{\bullet}} - \Delta_f H_{ArOR} + \Delta D_{corr}$$

where ΔD_{corr} is a correction for the effect of the cyano group, 0.15 eV, estimated from a correlation between the bond dissociation energies of phenyl ethers with σ^+ Hammet coefficients.[23]

In the absence of product cluster, we may apply eq 8 to compute the activation free energies predicted by the model. For this, we need, in addition to the driving force data, the values of E^*_{AB} and E^*_A. For E^*_{AB}, the B3LYP value computed in the

(20) Hapiot, P.; Pinson, J.; Yousfi, N. *New J. Chem.* **1992**, *16*, 877.
(21) (a) Benson, S. N. *Thermochemical Kinetics*; Wiley: New York, 1976. (b) *Handbook of Chemistry and Physics*, 72nd ed.; CRC: Cleveland, OH, 1991−1992; pp 9−121.
(22) Obtained from a frequency calculation (at the B3LYP/6-31G* level) on the optimized structure of the phenolate radical.
(23) Pratt, D. A.; de Heer, M. I.; Mulder, P.; Ingold, K. U. *J. Am. Chem. Soc.* **2001**, *123*, 5518.

Table 3. Estimation of E_A^* as a Function of the Method and Basis Set

method/ basis set	B3LYP/6-31G*	MP2/6-31G*	MP2/6-31+G*	MP2/6-311+G*
E_A^* (eV)	2.92	3.35	3.36	3.37
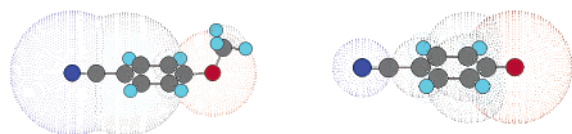
Figure 10. Spherical representation of the charge borne by each atom (from B3LYP/6-31G* calculations). The percentage of charge borne by a given atom is proportional to the radius of the sphere.

preceding section, 1.83 eV, may be used. For E_A^*, we have refined the B3LYP value by examining how it depends on the method and the basis set (Table 3). The average value, 3.215 eV, was finally retained.

The two full lines in Figure 9 represent the predictions of the model for two bracketing values of the solvent reorganization energy, $\lambda_0 = 0.4$ and 0.8 eV, for the lower and upper line, respectively. The discussion of whether such values of λ_0 are reasonable constitutes the final stage of the evaluation of the model. Solvent reorganization results from the intramolecular charge transfer that accompanies the homolytic cleavage. This is illustrated in Figure 10, which represents the distribution of the negative charge in the anion radical of 4-cyanophenyl methyl ether and in the 4-cyanophenyl oxide anion.

Initially, ca. 75% of the negative charge stands on the cyano group and on the neighboring carbon atom of phenyl group, the remaining charge being essentially located on the oxygen-alkyl part of the molecule. In the final anion, only 25% of the charge remains on the cyano group, while ca. 75% of the negative charge is on the oxygen atom and also partially on the phenyl group. The cleavage therefore entails the transfer corresponding to one-half of an electronic charge between these two portions of the molecule. Applying the Marcus charging process,[2c] one obtains the following estimate of the solvent reorganization energy.

$$\lambda_0 = \frac{N_A(\delta e_0)^2}{4\pi\epsilon_0}\left(\frac{1}{\epsilon_{op}} - \frac{1}{\epsilon_s}\right)\left(\frac{1}{2a_1} + \frac{1}{2a_2} - \frac{1}{d}\right)$$

(N_A, Avogadro's number; ϵ_0, permittivity of vacuum). δe_0 is the charge transferred, and ϵ_{op} and ϵ_s are the optical and static dielectric constants of the solvent, respectively. a_1 and a_2 are the radii of the two portions of the molecule exchanging charge, and d is the distance between their centers. In the present case, $a_1 = a_2 = 1.5$ Å, $d = 1$ Å, $\epsilon_{op} = 2.04$, and $\epsilon_s = 36.7$.[24] We thus obtain, as an approximate estimation, $\lambda_0 = 0.42$ eV, a value of the same order as those used for the simulation in Figure 9,

pointing therefore to the conclusion that the predictions of the model agree satisfactorily with experiment.

Conclusions

The main conclusions emerging from the above discussion are as follows.

(i) Activation barriers in the exothermic homolytic cleavage of radicals or ion radicals result from the intramolecular nuclear reorganization attending the transfer of one electron from a π^* to a σ^* orbital.

(ii) A two-state model may thus be devised, which, after inclusion of the bond cleavage and formation as Morse curves in the normal-mode analysis, leads to a simple quadratic activation driving force relationship. The two main ingredients of the intrinsic barrier are the triplet excitation energy of the leaving group and the $\pi^* \rightarrow \sigma^*$ excitation energy in the starting radical or ion radical.

Quantum Chemical Calculation Methodology

All of the calculations were performed with the Gaussian 98 series of programs.[25] Different methods were used: DFT (B3LYP) or Hartree–Fock with Möller–Plesset perturbation (MP2). The 6-31G* basis set was used unless otherwise stated. Minimum energy structures were fully optimized unless geometrical constraints were applied. Frequency calculations were made at the fully optimized geometries to verify that the structures were minima (no imaginary frequencies) or saddle point (one imaginary frequency). At a given level of theory, the activation barrier $\Delta U_{abi}^{\ddagger}$ was calculated as the electronic energy difference between the saddle point and the minimum structures. The nature of the reactant and products linked to transition states was assigned by the intrinsic reaction coordinate (IRC) method[26] at the same level of calculation as that used for saddle point characterization. IRCs have been determined in mass-weighted internal coordinates with a step size of 0.05 or 0.1 in au. Calculated bond dissociation energies were obtained from electronic energies only. Triplet excited states energies were calculated using the CIS method[27] for calculations at the MP2 level and the TD method[28] for calculations at the B3LYP level. Molecular orbitals were obtained using the cube method with 40 points per "side".

Supporting Information Available: Construction of orbitals and of orbital correlation diagrams. Normal coordinates for cleavage. Normal coordinates and interaction between fragments (PDF). This material is available free of charge via the Internet at http://pubs.acs.org.

JA027287F

(24) Kojima, H.; Bard, A. J. *J. Am. Chem. Soc.* **1975**, *97*, 6317.

(25) Frisch, M. J.; Trucks, G. W.; Schlegel, H. B.; Scuseria, G. E.; Robb, M. A.; Cheeseman, J. R.; Zakrzewski, V. G.; Montgomery, J. A., Jr.; Stratmann, R. E.; Burant, J. C.; Dapprich, S.; Millam, J. M.; Daniels, A. D.; Kudin, K. N.; Strain, M. C.; Farkas, O.; Tomasi, J.; Barone, V.; Cossi, M.; Cammi, R.; Mennucci, B.; Pomelli, C.; Adamo, C.; Clifford, S.; Ochterski, J.; Petersson, G. A.; Ayala, P. Y.; Cui, Q.; Morokuma, K.; Malick, D. K.; Rabuck, A. D.; Raghavachari, K.; Foresman, J. B.; Cioslowski, J.; Ortiz, J. V.; Stefanov, B. B.; Liu, G.; Liashenko, A.; Piskorz, P.; Komaromi, I.; Gomperts, R.; Martin, R. L.; Fox, D. J.; Keith, T.; Al-Laham, M. A.; Peng, C. Y.; Nanayakkara, A.; Gonzalez, C.; Challacombe, M.; Gill, P. M. W.; Johnson, B. G.; Chen, W.; Wong, M. W.; Andres, J. L.; Head-Gordon, M.; Replogle, E. S.; Pople, J. A. *Gaussian 98*, revision A.1; Gaussian, Inc.: Pittsburgh, PA, 1998.

(26) Gonzalez, C.; Schlegel, H. B. *J. Phys. Chem.* **1990**, *94*, 5523.

(27) Foresman, J. B.; Head-Gordon, M.; Pople, J. A.; Frisch, M. J. *J. Phys. Chem.* **1992**, *96*, 135.

(28) Casida, M. E.; Jamorski, C.; Casida, K. C.; Salahub, D. R. *J. Chem. Phys.* **1998**, *108*, 4439.